Precambrian Research 313 (2018) 134–147

Contents lists available at ScienceDirect

Precambrian Research

journal homepage: www.elsevier.com/locate/precamres

Did anoxia terminate Ediacaran benthic communities? Evidence from early diagenesis

Rachel Wood[a,*], Frederick Bowyer[a], Amelia Penny[a], Simon W. Poulton[b]

[a] School of GeoSciences, University of Edinburgh, James Hutton Road, Edinburgh EH9 3FE, UK
[b] School of Earth and Environment, University of Leeds, Leeds LS2 9JT, UK

ARTICLE INFO

Keywords:
Ediacaran
Redox
Reefs
Early marine cements
Dolomite

ABSTRACT

The Ediacaran oceanic redox landscape was heterogeneous, where many basins had a shallow and highly dynamic chemocline above anoxic (ferruginous or euxinic) or low oxygen (manganous) waters. Seawater mMg/Ca ratio was also high, promoting early diagenetic dolomitisation. How the benthos responded to these conditions is fundamental to understanding their ecological dynamics. Here we utilise redox sensitive elements in early marine carbonate cements to investigate possible water column redox controls on the distribution and growth of the oldest metazoan communities.

Skeletal communities in the Zaris Sub-Basin of the Nama Group, Namibia (~550–547 Ma), grew in shallow waters where fine-grained carbonate sediment often shows evidence of early dolomitisation. Mid-ramp *Cloudina* reefs are composed of open, highly porous structures that formed multiple, successive assemblages. Each assemblage is terminated by thin (< 1 mm), layers of dolomicrite sediment and dolomite cement. All dolomitic lithologies in the Nama Group analysed via Fe speciation suggest precipitation under anoxic ferruginous water column conditions.

Reef cements show a paragenetic sequence from synsedimentary to early marine cement and final burial, which we infer were precipitated under dynamic redox conditions. First, acicular pseudomorphed aragonite cement formed under oxic conditions (low Fe and Mn). Next, the presence of iron-rich dolomicrite sediment, often associated with a recrystallised ferroan dolomite crust, suggests that originally aragonitic or calcitic sediment and a high-Mg precursor cement were preferentially dolomitised. Dolomitisation may have been enhanced either via upwelling of deeper water, anoxic, ferruginous seawater, or by later fluid remobilisation from adjacent shales. A following Mn-rich calcite cement is inferred to be early marine due to its inclusion-rich, fibrous form and well-preserved CL zonation. The final blocky cement precipitated under oxic conditions, probably during shallow burial.

The cements likely record a general shallow to deeper water transect, from oxic shallow waters to low oxygen manganous waters, then to oxic, shallow burial conditions. We hypothesize that *Cloudina* reef communities were terminated by episodic sediment incursions during short-term, transgressive cycles, possibly accompanied by upwelled, anoxic, ferruginous and dolomitising waters, although the timing for this is poorly constrained. More generally, such incursions may have terminated Ediacaran benthic communities that grew close to the chemocline.

1. Introduction

Although metazoans did not come to ecological dominance until the early Cambrian, key ecological innovations appeared in the terminal Ediacaran, including biomineralization, reef-building, bilaterian burrowing, and macro-predation (Bengtson and Zhao, 1992; Knoll, 2003; Penny et al., 2014; Buatois et al., 2018). These evolutionary step-changes occurred in a globally heterogeneous redox landscape characterised by redox-stratified oceans and a highly dynamic chemocline (e.g. Lyons et al., 2014; Wood et al., 2015; Kendall et al., 2015). Redox instability continued long after the first appearance of probable metazoans, skeletal hard parts and metazoan reefs (Bowyer et al., 2017).

In addition, there is evidence that early marine Fe-rich dolomite precipitation dominated deeper waters in some late Ediacaran oceans, implying that not only was much of the water column ferruginous and anoxic, but may also have contained elevated Mg/Ca ratio (Wood et al., 2016; Hood and Wallace, 2018). Mimetic preservation by dolomite (i.e., retention of original crystallographic orientation) of original

* Corresponding author.
E-mail address: Rachel.Wood@ed.ac.uk (R. Wood).

https://doi.org/10.1016/j.precamres.2018.05.011
Received 15 January 2018; Received in revised form 29 April 2018; Accepted 10 May 2018
Available online 19 May 2018
0301-9268/ © 2018 The Authors. Published by Elsevier B.V. This is an open access article under the CC BY license (http://creativecommons.org/licenses/BY/4.0/).

aragonite and/or high-Mg calcite (HMC) grains (Tucker, 1982; Corsetti et al., 2006), as well as the presence of well-preserved dolomite cements, suggests that early marine dolomite precipitation dominated Cryogenian to early Ediacaran oceans (ca. 740–630 Ma; Hood and Wallace, 2015) and locally in the terminal Ediacaran (~550 Ma; Wood et al., 2016). This has been inferred to be due to widespread low-oxygen or stratified oceans and high-Mg/Ca seawater (Hardie, 2003; Hood et al., 2011; Hood and Wallace, 2018). The presence of high iron (ferroan) concentrations in early dolomite cements (Hood and Wallace, 2015), and ferroan dolomite concretions and iron speciation from shales further indicates that these oceans were anoxic and ferruginous (Canfield et al., 2008; Planavsky et al., 2011; Poulton and Canfield, 2011; Spence et al., 2016). Dramatically enhanced continental weathering occurred during the Neoproterozoic, creating a marked increase in carbonate deposition inferred to be due to a substantial input of Ca^{2+} into seawater (Peters and Gaines, 2012). Fluid inclusion data confirm that seawater Ca^{2+} increased markedly and Mg^{2+} declined slightly during the Ediacaran to early Cambrian, so progressively lowering mMg/Ca by the early Cambrian (Brennan et al., 2004).

The Ediacaran skeletal macrobiota were restricted to probably discontinuous habitable areas of well-oxygenated waters above the chemocline (Wood et al., 2015; Tostevin et al., 2016). The role of dynamic redox conditions in relation to the nature of the earliest metazoan benthos is therefore fundamental to understanding the ecological dynamics of the first metazoan communities. However, most bulk-rock geochemical techniques provide an indication of the dominant redox condition during sedimentation over geological rather than ecological timescales, and thus rapid fluctuations in water column redox conditions are seldom recorded. For example, in the lower Nama Group, Namibia, and the Windermere Supergroup, Canada, local palaeoredox indicators show pervasive anoxic signatures despite the presence of in-situ benthic communities of inferred metazoans (Johnston et al., 2013; Wood et al., 2015; Sperling et al., 2015a,b; Tostevin et al., 2016). This is suggestive of opportunistic benthic colonization during periods of transient oxygenation with episodic encroachment of anoxic waters beneath a very shallow, fluctuating chemocline (Wood et al., 2015).

The unusual chemical state of Ediacaran oceans will be manifest in the record of early marine cements. Here we consider the petrography, trace element and stable isotope composition of varied carbonate cements in metazoan reefs from the late Ediacaran Nama Group, Namibia. The use of early marine cements allows high-resolution reconstruction of the evolution of seawater-sourced pore fluids in shallow carbonate settings (Nothdurft et al., 2004; Della Porta et al., 2015; Hood and Wallace, 2015; Wallace et al., 2017). This is of particular utility in the Ediacaran, as shallow shelf carbonates host the highest diversity of skeletal metazoans. Dolomite is also common in the Nama Group, and all dolomitic lithologies analysed via Fe speciation suggest precipitation under anoxic water column conditions (Wood et al., 2015). Therefore, we also consider evidence that dolomitisation may indicate transient anoxic seawater conditions, which in turn may have structured the longevity and ecology of Ediacaran skeletal communities.

1.1. Petrographic evidence for Neoproterozoic marine dolomite

In order to distinguish cements as marine, they must fulfil criteria that indicate precipitation from seawater-sourced fluids (Davies, 1977; Hood and Wallace, 2012, 2018). These include 1) an isopachous, pore-lining fabric of fibrous and inclusion-rich crystals oriented normal to cavity walls, 2) cements directly intergrown with or succeeded by marine geopetal sediments, and 3) cements truncated by other early-forming features such as neptunian fractures.

That some late Neoproterozoic carbonate cements represent marine dolomite is based upon crystallographic character and how dolomite replaces pre-existing carbonate fabrics (Tucker, 1983; Hood and Wallace, 2012, 2015, 2018). Carbonate cements precipitated in seawater will usually be length-fast (with a low angle between the crystal c-axis and the fastest growth vector), and grow rapidly either as acicular, aragonite (orthorhombic) crystals with blunt terminations, or more slowly as calcite (trigonal) crystals with either acute rhombohedral, or scalenohedral form (Folk, 1974; Berner, 1975). By contrast, sparry calcite will be length-slow (with a high angle between the crystal c-axis and the fastest growth vector) and is most commonly precipitated as late stage (burial) pore-occluding cement where low Mg/Ca solutions and negligible contamination by Mg^{2+} ions does not inhibit growth perpendicular to the c-axis (Folk, 1974; Folk and Land, 1975). Marine dolomite cements (which do not naturally occur in seawater today) always show a length-slow character and commonly conform to three crystal forms termed 'radial slow', 'radiaxial slow' and 'fascicular slow' dolomite (Hood et al., 2011; Hood and Wallace, 2012, 2015, 2018).

Dolomitisation of a calcite cement precursor will be syntaxial and preserve the original character and optical continuity of calcite as a consequence of the common crystal form (trigonal rhombohedra) shared by both dolomite and calcite (Hood and Wallace, 2012). By contrast, dolomitisation of an aragonite precursor will only crudely preserve the original aragonitic fabric due to the contrast in crystal form between aragonite (orthorhombic) and dolomite (trigonal) (Hood and Wallace, 2012). As such, primary marine dolomite is represented by an isopachous and inclusion-rich cavity-lining cement, which retains its original length-slow character (Hood and Wallace, 2012, 2018).

2. The Ediacaran Nama Group, Namibia

2.1. Geological setting

The Nama Group (~550–541 Ma) is a terminal Ediacaran succession of highly fossiliferous mixed clastics and carbonates ranging from supratidal to outer ramp settings with varying hydrodynamic conditions (Grotzinger and Miller, 2008). The Nama Group was deposited across the Zaris and Witputs sub-basins separated by the Osis Arch (Fig. 1A), and the strata have been correlated using sequence stratigraphy, chemostratigraphy, and dated ash beds (Saylor et al., 1995, 1998; Grotzinger et al., 1995).

We consider in situ *Cloudina* reefs at Driedoornvlagte reef complex (Penny et al., 2014; Wood and Curtis, 2015), from the far north of the Zaris subbasin (Fig. 1A), which formed during deposition of from the Omkyk Member, Kuibis Subgroup (Fig. 1B). Driedoornvlagte is an isolated carbonate platform approximately 10 km in length and ~500 m thick that grew in a high-energy, mid-ramp setting (Smith, 1998; Adams et al., 2004). Uranium-lead chronology of an ash bed in the immediately overlying lower Hoogland Member (upper Kuibis Subgroup) yields an age of 547.32 ± 0.65 Ma (Grotzinger et al., 1995; Schmitz, 2012).

2.2. Water column redox

Low total iron (FeT) in carbonates, normal marine Fe/Al in shales and carbonate, and the presence of negative cerium anomalies in carbonates indicates an oxic environment, suggesting that reef growth at Driedoornvlagte was into a dominantly oxic water column (Wood et al., 2015; Tostevin et al., 2016; Bowyer et al., 2017). Sequence stratigraphy shows that reef growth took place during a long-lived transgression (Adams et al., 2004). However, adjacent deeper waters were characterised by either low-oxygen manganous conditions, or anoxic ferruginous conditions (Wood et al., 2015; Tostevin et al., 2016; Bowyer et al., 2017). A very shallow oxycline persisted throughout deposition of shelf grainstones during the Lower Omkyk Member (OS1), as evident from anoxic ferruginous waters during transgression, to manganous conditions during the highstand systems tract (Wood et al., 2015). By contrast, early Upper Omkyk Member (OS2) sediments record a transition to well-oxygenated conditions, and reef growth at Driedoornvlagte took place during an interval of stable oxia. Similarly, oxic water column conditions dominated time-equivalent deposition at more

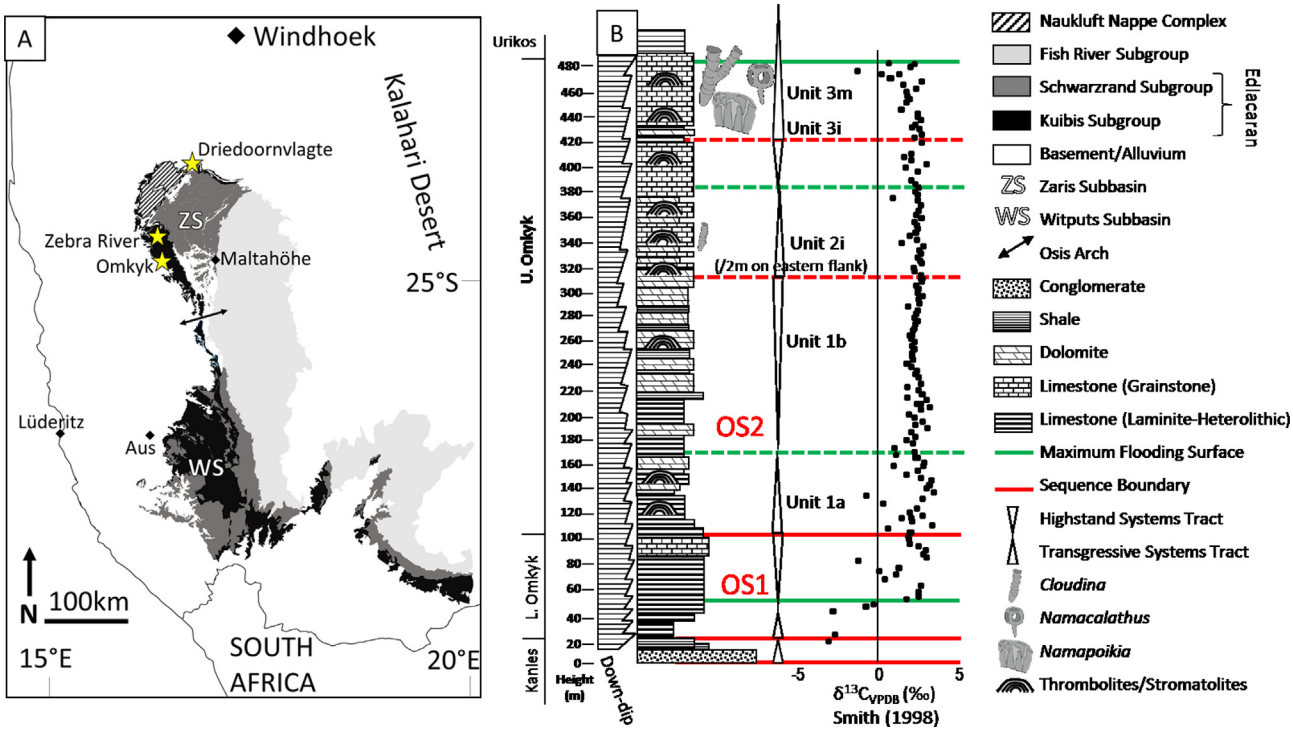

Fig. 1. Location and stratigraphic setting of the Nama Group, Namibia. (A) Simplified map showing geological setting, subgroups, and sub-basins of the late Ediacaran to early Cambrian Nama Group of southern Namibia, with the location of Driedoornvlagte reef, Zebra River and Omkyk. (B) Stratigraphic log of the Omkyk Member at the Driedoornvlagte isolated carbonate platform showing concurrent slope and basinal shale and overlying shale of the Urikos Member (after Adams et al., 2004) with carbon isotope chemostratigraphy (Smith, 1998) and metazoan fossil distribution.

proximal mid-ramp sites, including Zebra River where smaller, biostromal reefs also formed (Wood et al., 2015).

By contrast, pulsed ferruginous conditions are recorded in inner ramp settings, which may reflect either development of sluggish circulation and elevated productivity, or upwelling of anoxic deep water during transgression (Wood et al., 2015; Bowyer et al., 2017). Ce anomaly data indicate episodic incursion of manganous waters at shallow water depths at inner ramp sites, and at intermediate depths at slightly deeper mid-ramp settings (Tostevin et al., 2016). Limestone and dolomite lithologies are common in the Nama Group, and while limestone shows both oxic and anoxic redox signatures via Fe speciation, all dolomite analysed suggests precipitation under anoxic water column conditions (Wood et al., 2015). Whilst early dolomitisation may result in minor increase in the ratio of Fe_{HR}/Fe_T, this is not expected to yield values > 0.38, i.e. ratios indicative of anoxia (Clarkson et al., 2014). Dolomitic lithologies of the Nama Group show Fe_T from 0.31 to 2.38 wt % and, where Fe_T > 0.5 wt%, Fe_{HR}/Fe_T from 0.29 to 1. These are strongly suggestive of formation within an anoxic and iron-rich water column (Wood et al., 2015).

Marine transgressions show repetitive shoaling of the oxycline, and general reef growth may have been terminated by clastic influx and the development of anoxic ferruginous conditions with deposition of the overlying transgressive Urikos Member shales on the deep, outer shelf at Driedoornvlagte (Adams et al., 2004; Bowyer et al., 2017). A broadly synchronous, but short-lived, phase of anoxia is documented across the mid to inner ramp at the maximum flooding surface of the large scale transgressive systems tract (at the base of parasequence 4 of Adams et al., 2004, 2005), contemporaneous with the Urikos shale (Bowyer et al., 2017).

2.3. Architecture and fabric of the Driedoornvlagte reef complex

The notably expanded stratigraphic thickness of OS2 at Driedoornvlagte relative to shallower sections is inferred to be due to foreland basin subsidence in proximity to the Damara orogen (Smith, 1998; Grotzinger and Miller, 2008). Driedoornvlagte carbonate platform growth kept-up with subsidence-induced relative sea level rise during deposition of the OS2, but was eventually drowned by fine, basinal siliciclastics of the Urikos Member, equivalent to carbonate production of OS2 Units 4 and 5 in shallower sections to the south (Smith, 1998; Adams et al., 2004, 2005; Dibenedetto and Grotzinger, 2005).

The carbonate build-up of OS2 is interpreted to record 3 cycles (Units 1–3) of relative sea level change, each of which is represented by sequentially expanded stratigraphic horizons as a consequence of increasing subsidence during deposition (Figs. 1b and 2) (Adams et al., 2004). Microbial-metazoan reefs at Driedoornvlagte grew in association with coalesced thrombolite mounds of the final cycle of reef growth (Unit 3 m), representing a ~50 m thick transgressive succession which formed in a shallow subtidal setting immediately prior to drowning (Grotzinger et al., 1995; Adams et al., 2004). There have been no recorded occurrences of evaporite pseudomorphs, karstification or other features indicative of subaerial exposure or evaporitic conditions. The inferred accommodation increase during deposition of Unit 3 m is based upon an observed increase in size of coalesced thrombolite-stromatolite mounds, and the formation of synsedimentary fissures and collapse breccias (Adams et al., 2004).

In Unit 3 m, *Cloudina* reefs are broadly associated with *Namacalathus* communities, and *Namapoikia*, which preferentially inhabited synsedimentary fissures (Wood et al., 2002; Wood and Curtis, 2015). Although the presence of *Cloudina* reefs has been disputed (Mehra and Maloof, 2018), in-situ reef growth is confirmed by: a) the mutual attachment of *Cloudina* individuals by 'meniscus' skeletal structures in life position together to form frameworks, and b) decimeter-scale cement-filled, reef framework cavities (Penny et al., 2014; Wood and Curtis, 2015).

Reefs were highly porous structures, where pore space between adjacent individuals and framework cavities being filled dominantly

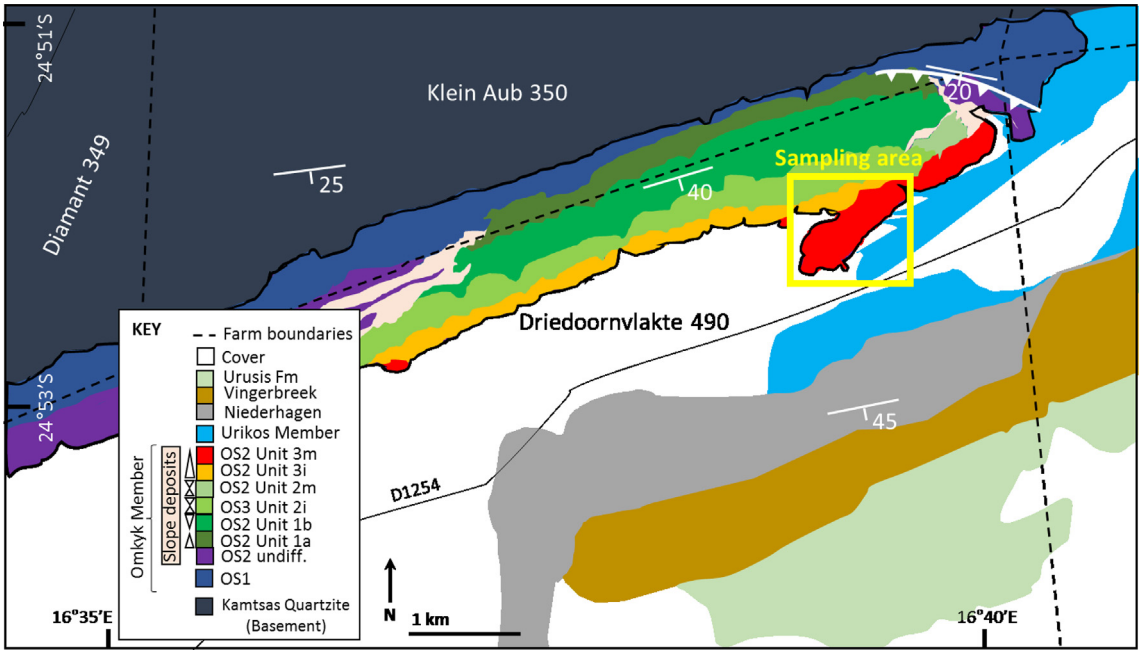

Fig. 2. Geological map of the Driedoornvlagte isolated carbonate platform with the position of the sampling area in Unit 3 m highlighted by the yellow box (after Adams et al., 2004).

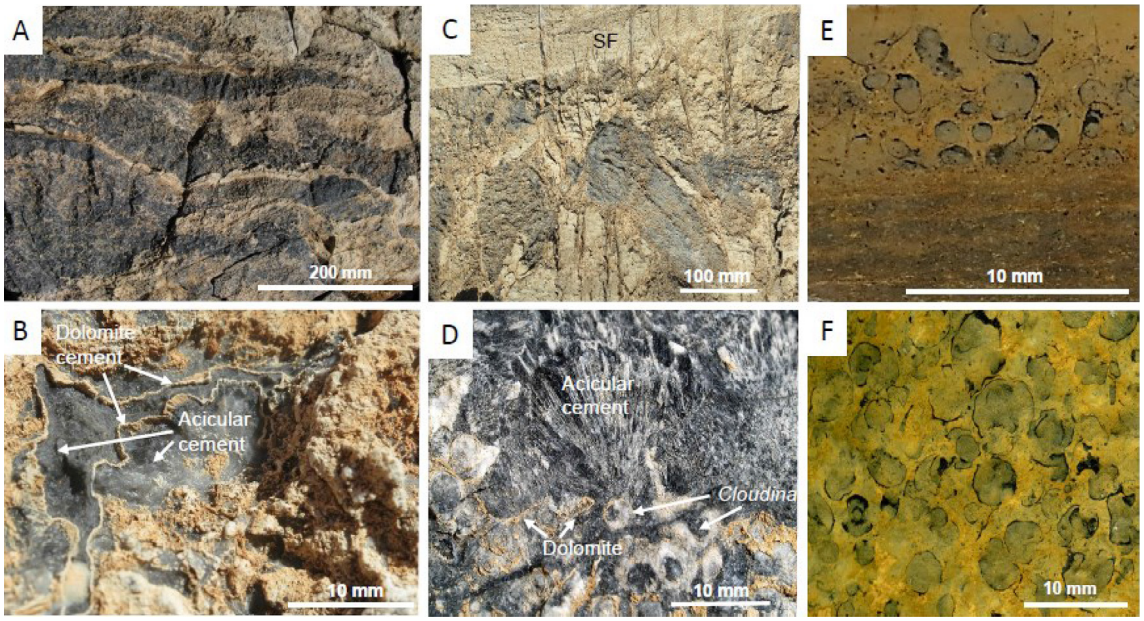

Fig. 3. Field photographs of Ediacaran communities associate with dolomite. (A) *Cloudina* reef showing repeated assemblages of *Cloudina* reef terminated by light brown dolomitised sediment. (B) Reef void filled with acicular cement encrusted by dolomite cement. (C) Collapse breccia showing limestone and dolomite clasts within a dolomicrite matrix, truncated by a synsedimentary fissure (SF). (D) Recrystallised *Cloudina* individuals encrusted by acicular cement. (E and F) Inner ramp *Namacalathus* assemblage showing dolomitisation of surrounding micritic sediment, but retention of limestone within the *Namacalathus* cups. (E) Longitudinal polished section. (F) Bedding plane surface.

with acicular calcite cements (Fig. 3B,D), and a small volume of microbialite and geopetal sediment (Grotzinger et al., 2003; Penny et al., 2014; Wood and Curtis, 2015).

Some *Cloudina* reefs have been interpreted as composite, composed of up to 20 repeated lens-shaped units or assemblages, 10–30 cm in height and up to 3 m in length (Fig. 3A; Wood et al., 2017). The upper part of each units grades into a layer 5–32 mm thick, which is preferentially dolomitised and composed of an increasing density of microthrombolitic clots, stromatolitic laminae, or thin (< 1 mm) discontinuous to highly laterally continuous layers of sediment with dolomite cement crusts (Figs. 3A and 4A). The final layers, commonly composed of geopetal micrite sediment, mark a sharp boundary before growth of the succeeding unit, and may be erosionally-truncated (Wood et al., 2017).

At Driedoornvlagte, the reef complex is dolomitised but the surrounding stratigraphy, including shales, is generally un-dolomitised. Driedoornvlagte slope lithologies and adjacent basinal deposits also commonly contain dolomitised grainstones or mudstones, respectively (Adams et al., 2004). In particular, dolomitized mudstone rip-up clasts are found at the bases of grainstone beds, and intraclast breccias found

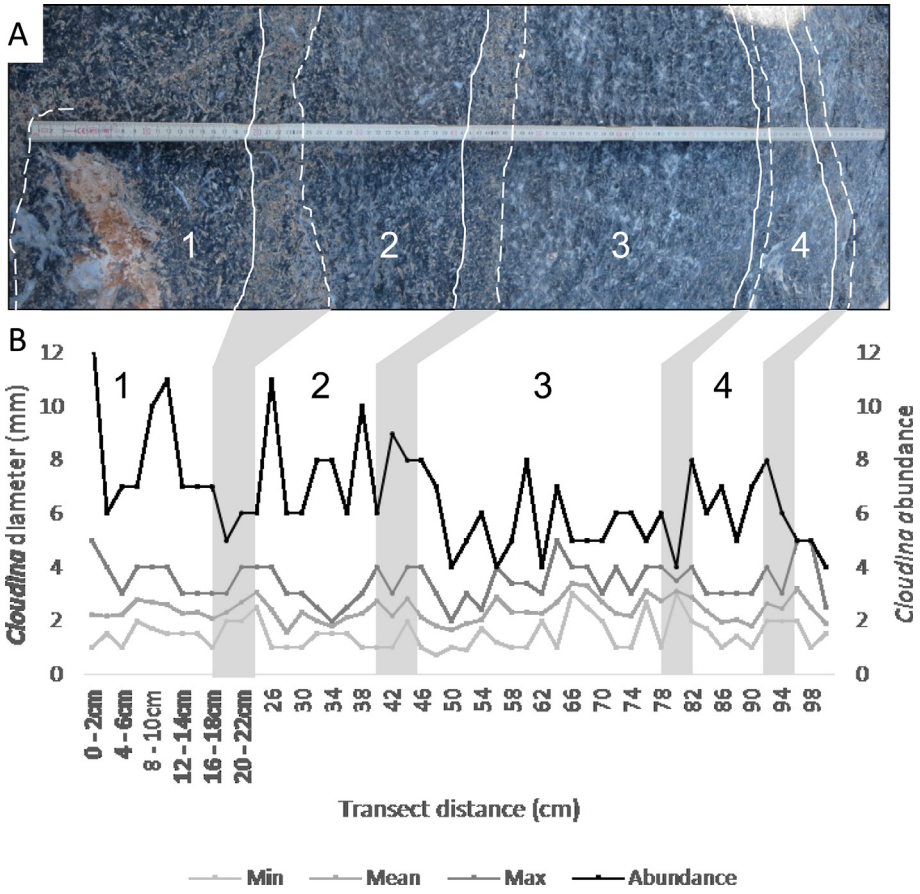

Fig. 4. Size distribution and abundance of *Cloudina* through a tangential transect at Driedoornvlagte reef. (A) Field image of transect showing successively. Modified from Wood et al., 2017.

in basin settings containing dolomitised grainstone clasts within a dolomitized, muddy matrix (Adams et al., 2004).

Collapse breccias often consist of angular limestone and dolomite clasts within a dolomicrite sediment matrix, which can be truncated by synsedimentary fissures (Fig. 3C). Abundant dolomite cement is also recognised in the field, where it encrusts acicular cements within voids in addition to *Cloudina* individuals (Fig. 3B and D). Dolomite cement increases in volume from the base to the top of each assemblage, and field observations suggest that its occurrence was controlled by the available pore space for precipitation after growth of acicular cement.

In a ~1 m transect taken at 20 mm intervals though a *Cloudina* reef (Fig. 4A), the size of *Cloudina* varies through each successive community, including an increase in *Cloudina* diameter towards the top of each assemblage (Fig. 4B; Wood et al., 2017). Abundance (density), however, shows no correlation with position within a community, but does show an overall general decrease through the transect (Fig. 4B). Environmental controls on *Cloudina* size are unknown, and may include cyclical changes in nutrient levels, water depth, hydrodynamic energy, space availability, or carbonate supersaturation.

In the Nama Group, marine transgressions led to a shoaling of the oxycline (Bowyer et al., 2017). Here, we hypothesize that termination of Ediacaran skeletal communities across the ramp may be due to the flooding of shoaling, anoxic waters. We test this by considering the succession of calcite and dolomite cements, and sediments.

3. Materials and methods

Large hand samples were taken from multiple *Cloudina* reefs from the ~50 m thick mixed microbial-metazoan Unit 3 m on the southeast flank of the carbonate build-up on Farm Driedoornvlagte (Fig. 2). The palaeo-horizontal was defined by micritic geopetal sediments within and around *Cloudina* individuals.

Thin sections (75 × 50 mm) were etched with 0.2 M hydrochloric acid for 10 s followed by staining with a mixed solution of Alizarin Red S and Potassium ferricyanide in 0.2 M HCl for approximately 30 s before rinsing with deionised water (Dickson, 1965).

We examined polished thin sections under a Cathodoluminescence Cold Cathode CITL 8200 MK3A mounted on a Nikon optiphot microscope to identify differing luminescence (Habermann et al. 1996; 1998; Mason and Mariano, 1990). All cements were analysed for major element concentrations (Fe, Ca, Mg, Mn, Sr) using a Cameca SX100 Electron Microprobe at the University of Edinburgh with an 80 s count time, a beam diameter of 3 μm, an accelerating voltage of 15 kV, and a beam current of 35 nA.

Powders of sample size 0.03–0.2 mg were removed for isotope analysis from thin sections using a tungsten steel needle under a Leica 240 microscope. Powders were dissolved at 25 °C with 100% phosphoric acid followed by conventional mass spectrometry using a Thermo Electron Delta+ Advantage. Results are reported as deviations from the VPDB standard (‰) and precision was measured at a level better than 0.1‰ for $\delta^{13}C$ and $\delta^{18}O$.

X-ray diffraction was undertaken on one sample of mixed composition (calcite, dolomite and dolomitised sediment). Dolomite stoichiometry was obtained on via the 104 peak shift XRD method (Lumsden and Chimahusky, 1980), using a weighted mean incident wavelength for CuKα radiation of 1.541838 Å and the $^{d}104$ peak at a 2θ angle of 30.9°.

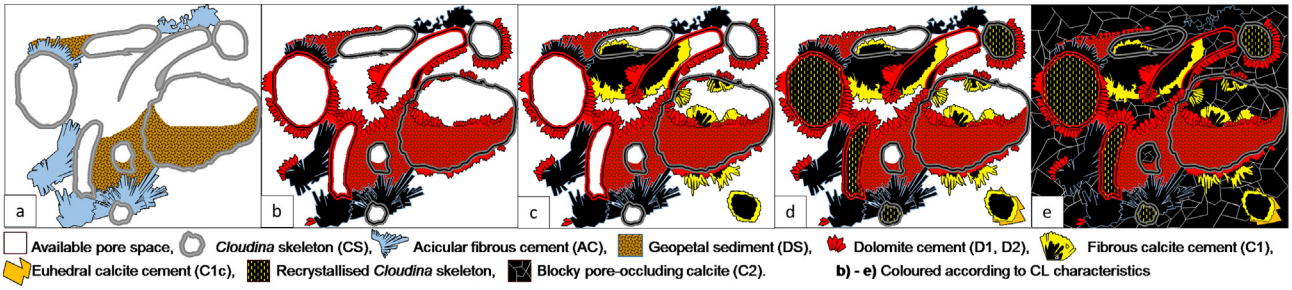

Fig. 5. Paragenetic sequence. (A) *Cloudina*, acicular cement (AC), and geopetal sediment (DS); (B) Dolomitisation of geopetal sediment (DS), dolomitisation of *Cloudina* (D1), and precipitation of dolomite cement (D2); (C) Fibrous calcite growth (C1a/b); (D) Recrystallisation of *Cloudina* skeleton plus euhedral cement growth (C1c); (E) Blocky pore-occluding calcite cement (C2).

4. Results

4.1. Distribution of cements, petrography and elemental geochemistry

Driedoornvlagte *Cloudina* reefs show a consistent diagenetic paragenetic sequence of six successive cement generations (Fig. 5), each with distinct petrographic and cathodoluminescence characteristics, and Fe, Mn and Sr concentrations (Table 1 and Supplementary data) as described below.

Cloudina skeletons (CS) are preserved either as neomorphic calcite or finely crystalline calcite, in some cases with microdolomite inclusions, or can be completely dolomitised (Fig. 6E). Where not dolomitised, Mn concentrations are up to 1130 ppm (mean 160 ppm; n = 48), and Fe concentrations reach 630 ppm (mean 140 ppm; n = 48). Sr concentrations reach up to 1600 ppm (mean 480 ppm; n = 48).

Large (up to 40 mm radius), volumetrically abundant acicular cements with square crystal terminations form botryoids (AC; Fig. 3D), which are pseudomorphed from aragonite (Grant 1990). These grow dominantly from *Cloudina* skeletons (Fig. 6B). AC also intergrew with geopetal sediment (Fig. 6A). Acicular cements are mainly non-luminescent (Fig. 7C and D), but some show patchy non-luminescence (Fig. 7C). Acicular cements are volumetrically most abundant in the lower to middle parts of each assemblage where they may occlude most or all pore space. Mn concentrations for the pseudomorphed botryoids are below detection limits (BDL) and Fe concentrations are close to detection limits (mean 150 ppm; n = 21). Sr concentrations are up to 6890 ppm (mean 1890 ppm; n = 21).

At the top of each *Cloudina* assemblages, thin (< 1 mm) layers of geopetal, internal dolomicritc sediment (DS) appear, commonly with a nonplanar texture (Sibley and Gregg, 1987; Fig. 6A and E). This sediment appears only in the upper parts of each assemblage, and often, but not always, terminates acicular cement growth (Fig. 6A). Geopetal sediments also commonly infill *Cloudina* individuals (Fig. 7A), and the elemental composition ranges of these sediments is indistinguishable from both the sediment that covers acicular cements and *Cloudina* skeletons. Dolomicritic sediment fill has elevated Fe (up to 6850 ppm, mean 1980 ppm, n = 52), and slightly elevated Mn (up to 1000 ppm, mean 220 ppm, n = 52). Sr reaches up to 720 ppm, mean 150 ppm (n = 52).

The microcrystalline skeletal structure of some *Cloudina* individuals has been partially or completely dolomitised (D1). D1 is mid-brown and inclusion-rich, with poorly preserved, often patchy, CL zonation (Fig. 7F). Pervasive recrystallisation of individual D1 crystals commonly obscures grain boundaries and original crystal width making measurement difficult but individual crystals are < 20 µm in length (Fig. 6E). D1 shows elevated Fe (up to 9750 ppm, mean 880 ppm, n = 38) and low Mn (up to 820 ppm, mean 120 ppm, n = 38). Sr reaches up to 720 ppm (mean 150 ppm; n = 38).

A thin isopachous, dolomite cement (D2) follows, which precipitates either vertically upon geopetal sediment as an upward-growing crust (Figs. 7A and 8D), or on D1 cement (Fig. 6D and E), or radially around *Cloudina* skeletons (Fig. 8C–G), or directly upon acicular cements (Fig. 7C and D). The D2 crust becomes most abundant in the upper parts of each assemblage where more pore space was available (i.e. less occlusion by acicular cements) but is also well developed in localised areas of shelter porosity beneath or within *Cloudina* individuals (e.g. Fig. 8D).

D2 is pale brown, inclusion-rich (Fig. 6D, E; 9A, C), and poor (patchy) (Fig. 7B–D), but with occasionally well-preserved CL zonation of usually dull zones that do not extend across crystal boundaries (Fig. 9B, D and F). D2 shows greater definition of growth zonation towards rhombic terminations (Fig. 9B, D and F). Where best preserved, individual crystals show unit extinction. D2 cement crystals largely show a unimodal size distribution (length ~250 µm, max width ~200 µm).

Fibrous D2 cements show a radial length-slow character (Fig. 9B and D) with obtuse rhombic crystal terminations, however in other areas D2 exhibits acute terminations indicative of a length-fast character (Fig. 9F). This difference in inferred crystallographic character may simply be a consequence of perspective whereby the plane of the thin section bisects length fast crystals at angles divergent from the c-axis (Dickson, 1983). In some rare instances, D2 cements contain cubic crystals with a maximum diameter of 20 µm, which display blue-violet luminescence under CL (Arrowed, Fig. 9G). These features are consistent with the presence of fluorite.

D2 also shows evidence for multiple phases of dissolution, particularly near crystal terminations (Arrowed, Fig. 7D, 9E). D2 also shows elevated Fe (up to 7020 ppm, mean 1440 ppm, n = 143) and low Mn (up to 840 ppm, mean 230 ppm, n = 143). Sr reaches up to 670 ppm (mean 130 ppm, n = 143).

The dolomite sampled is non-stoichiometric and calcic, with the XRD sample showing 47.33 mol% $MgCO_3$. Electronprobe data reveal a range of Mg/Ca from 0.40 to 0.66 (n = 184). There do not appear to be any uniform trends in Mg/Ca through individual dolomite cements from nucleation point of D1 to crystal termination of D2 (see Supplementary data).

D2 is post-dated by a calcite cement, C1 (Figs. 7 and 8). C1 is a cloudy, inclusion-rich low-Mg calcite cement, forming as length-fast scalenohedra (Figs. 7A, B; 8E, F). Individual crystals exhibit an average length-width ratio of 5:1 when the plane of the thin section bisects the crystal parallel to the c-axis. C1 cement is not isopachous but may grow either vertically upward or downwards from cavity ceilings and directly nucleate upon D2, skeletal *Cloudina* material or AC cements. C1 columnar scalenohedral cements invariably radiate from single points, forming bundles which, when cut perpendicular to the plane of the thin section, appear as rosettes with non-luminescent to patchy bright luminescent or non-luminescent columnar cores (C1a) and brightly luminescing rims (C1b) (Fig. 9G, H).

In C1a, Fe is low (up to 650 ppm, mean 180 ppm), as is Mn (up to 930 ppm, mean 240 ppm) and Sr is up to 1100 ppm, (mean 340 ppm) (n = 21). In C1b, Fe is low (up to 300 ppm, mean 130 ppm), Mn is notably elevated (up to 3700 ppm, mean 1750 ppm) and Sr is up to

Table 1
Elemental concentrations (ppm) of Fe, Mn, and Sr, and Mg/Ca and Mn/Sr for *Cloudina* and each component.

Component	Mg/Ca				Mn			Fe			Sr			Mn/Sr			
	Min	Max	Mean	Standard Deviation	Min (ppm)	Max (ppm)	Mean (ppm)	Standard Deviation	Min (ppm)	Max (ppm)	Mean (ppm)	Standard Deviation	Min (ppm)	Max (ppm)	Mean (ppm)	Standard Deviation	Min	Max	Mean	Standard Deviation
Acicular Cement (AC)	0.000	0.009	0.005	0.003	BDL	128	BDL	0.004	BDL	399	148	0.013	119	6889	1890	0.205	0.006	0.354	0.089	0.094
Cloudina Skeleton (CS)	0.003	0.078	0.014	0.036	BDL	1134	162	0.021	BDL	626	139	0.014	182	1607	475	0.026	0.002	2.161	0.374	0.442
Dolomitised Sediment (DS)	0.251	0.661	0.566	0.060	BDL	999	219	0.016	330	6848	1983	0.142	BDL	719	148	0.010	0.168	10.741	2.062	2.189
Dolomite 1 (D1)	0.469	0.661	0.573	0.042	BDL	818	120	0.020	BDL	9749	879	0.205	BDL	724	147	0.012	0.013	4.029	1.065	1.187
Dolomite 2 (D2)	0.395	0.648	0.567	0.043	BDL	845	228	0.017	BDL	7024	1435	0.162	BDL	670	134	0.009	0.042	28.333	2.927	4.355
Calcite 1 (C1a)	0.004	0.010	0.007	0.002	BDL	926	242	0.022	BDL	651	176	0.022	BDL	1093	343	0.030	0.025	6.600	1.580	1.763
Calcite 1 (C1b)	0.002	0.017	0.007	0.004	502	3703	1753	0.102	BDL	302	130	0.009	150	800	396	0.017	0.628	16.347	5.160	4.717
Calcite 1 (C1c)	0.005	0.005	0.005	0.000	396	405	400	0.001	BDL	BDL	BDL	0.007	406	556	481	0.011	0.728	0.975	0.852	0.175
Calcite 2 (C2)	0.001	0.024	0.007	0.006	BDL	199	BDL	0.006	BDL	378	BDL	0.012	BDL	4068	792	0.102	0.005	1.026	0.297	0.320

800 ppm, (mean 400 ppm) (n = 14). The non-luminescing zones of C1a and C1b are etched by dissolution (Fig. 8F).

Rarely, C1a/b is overgrown by a limpid euhedral calcite cement of moderate luminescence (C1c) (brighter than D1 and D2 but duller than C1b) which lacks inclusions but preserves fine CL zonation with only very minor variability in luminescence between growth zones (Fig. 7F). This cement sometimes appears as an epitaxial overgrowth of C1 (Fig. 7F) and invariably lacks evidence for dissolution at crystal terminations. C1c postdates all other diagenetic cements with the exception of the final pore occluding calcite precipitate discussed below and is characterised by iron below detection, low Mn (max 405 ppm, mean 400 ppm), and low Sr (max 550 ppm, mean 480 ppm) (n = 2).

All remaining pore space is occluded by a clear, low-Mg blocky calcite (C2) which most commonly shows straight extinction in cross polars but occasionally twinning and invariably shows non- to dull-luminescent zonation (Figs. 7A, F, 8E, F). Both Fe and Mn are below detection in C2 whilst Sr is up to 4070 ppm (mean 790 ppm) (n = 15). An additional volumetrically sparse component is represented by patchy non- to dull luminescent rhombic dolomite crystals of up to 250 μm in maximum length which appear to float within C2 or aggregate about zones of complex dissolution which display moderate luminescence similar to C1c. This phase has not been analysed.

Summarised elemental data reveal the distinctive elemental composition of the cements (Table 1). Acicular cements (AC) have high Sr concentrations, but low Fe and Mn. Non-dolomitised *Cloudina* skeleton (CS) has slightly elevated Sr concentrations, but low Fe and Mn. Dolomicrite sediment (DS), dolomitised *Cloudina* skeleton (D1) and dolomite cement (D2) have notably high Fe and low Mn and Sr. By contrast, calcite cement 1a (C1a) has low Fe, Mn and Sr, calcite cement 1b (C1b) has low Fe and Sr but high Mn, and calcite 1c (C1c) has low Mn, Fe and Sr. Calcite 2 (C2) records low Fe and Mn but slightly elevated Sr.

4.2. Carbon and oxygen isotopes

Cloudina skeleton (CS), thrombolite, and calcite spar cement (C2) show a narrow range of $\delta^{13}C_{PDB}$ from 1.67 to 2.36‰ (mean 2.10‰), and $\delta^{18}O_{PDB}$ from −9.94 to −4.09‰ (mean −7.37‰). Acicular cement shows a slightly wider range of $\delta^{13}C_{PDB}$ from 1.15 to 3.02‰ (mean 2.49‰), and similar values of $\delta^{18}O_{PDB,}$ from −10.99 to −6.63‰ (mean −8.40‰). Combined dolomitised sediment and dolomite cements show a slightly wider range of both $\delta^{13}C_{PDB}$ from −0.29 to 2.62‰ (mean 1.22‰), and $\delta^{18}O_{PDB,}$ from −11.60 to −4.15‰ (mean −8.19‰) (Fig. 10).

5. Discussion

5.1. Origin of calcite cements

Iron and manganese concentrations influence cathodoluminescence in marine carbonate cements, so providing constraints on the redox conditions for the pore fluids (Barnaby and Rimstidt, 1989; Hood and Wallace, 2015). Non-luminescent cements have low Fe and Mn; bright luminescent cements have high (activating) Mn values, but low Fe; and dull luminescent cements have moderate values of both Fe (quenching) and Mn. A non-luminescent, through bright, to dull luminescent stratigraphic progression is caused by carbonate precipitation in waters with decreasing Eh that are in equilibrium with poorly crystalline Fe–Mn oxides (Barnaby and Rimstidt, 1989). The overall Fe–Mn and cathodoluminescence behaviour of the Driedoornvlagte reef cements are similar to that observed in burial cement successions from Phanerozoic carbonates (e.g. Grover and Read, 1983).

Cathodoluminescence may also reveal fine growth zones within cements, which correspond to variable redox chemistry (Barnaby and Rimstidt, 1989). Recrystallisation or replacement by another mineral will destroy original cathodoluminescence zonation. The preservation of such delicate zonation, which does not extend beyond crystal

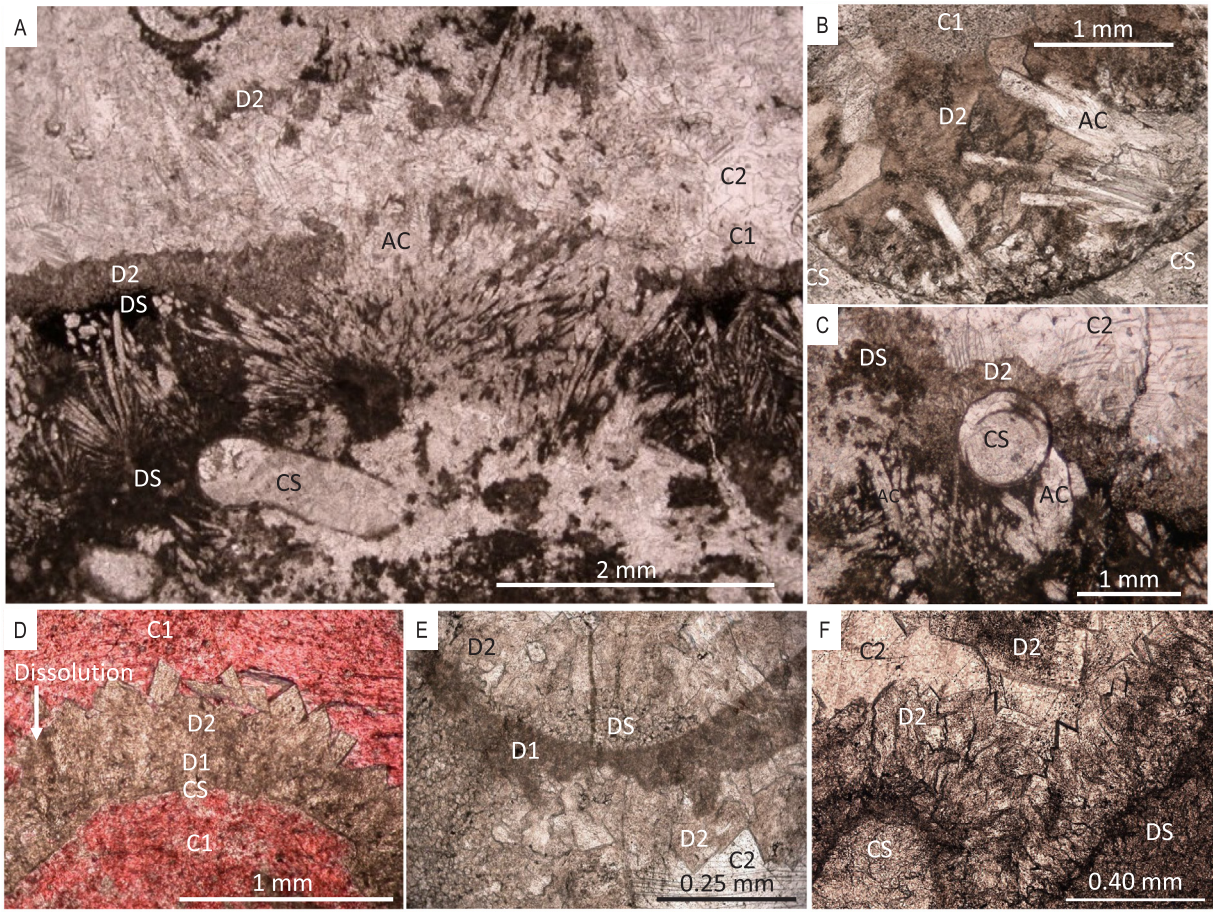

Fig. 6. Photomicrographs of cements in plane polarised light. Fibrous botryoidal cement nucleating on dolomitised sediment (A), and *Cloudina* skeleton (B). Dolomitised geopetal sediment commonly overlies acicular cement and *Cloudina* skeleton fragments (A, B, C, F). Inclusion-rich generation of isopachous dolomite cement encrusts a recrystallized *Cloudina* skeleton (D, F), succeeded by the second generation of dolomite cement (A, C, D–F), sometimes showing evidence for dissolution in section stained with Alizarin red (D). CS: *Cloudina* skeleton, AC: Acicular fibrous cement, DS: Dolomitised sediment, D1: Dolomite cement 1, D2: Dolomite cement 2, C1: Calcite cement 1, C2: Calcite cement 2.

boundaries, therefore indicates that cements are a product of primary growth. Zonation patterns are controlled by the crystal form of each cement type, and so reveal the direction of pore-filling crystal growth away from a substrate (Hood and Wallace, 2012, 2018).

The inclusion-rich, acicular cement (AC) is interpreted to represent an early marine precipitate of originally aragonitic mineralogy. The interpretation of an originally aragonitic mineralogy for AC is supported by the elevated Sr content (up to 6900 ppm), as previously reported at Driedoornvlagte by Grant (1990). The acicular, aragonite-precursor cement (AC) is commonly overlain by both geopetal dolomicrite sediment (DS) inferred to be of marine origin, and by *Cloudina* individuals, which either grew against or were deformed by acicular cement (Fig. 8A).

The general absence of clear CL zonation in the dolomite cements (D1 and D2) suggests recrystallisation after a precursor, but these cements are nonetheless distinct from both burial cements and coarsely recrystallised, dolomitic replacements (Whittaker et al., 1994; Corsetti et al., 2006). However, there are localised instances where the dolomite cement shows fine zonation, revealing a crystal form very similar to shorter, wedge-shaped marine dolomite cements of the older Karibib Formation, Northern Namibia, which also show greater definition of growth zonation towards rhombic terminations (Hood and Wallace, 2018).

The columnar length-fast character and scalenohedral form of C1 cement crystals when bisected parallel to the c-axis (e.g. Fig. 9H) suggest an original HMC mineralogy. Whilst there are no documented occurrences of geopetal sediment postdating C1 cements, the length-fast and inclusion-rich character and growth within shelter porosity, argues for C1 cement precipitation in pore fluids that were in open contact with seawater.

Current data do not adequately distinguish between individual episodes of alteration. Clear CL zonation in C1c and C2 may indicate that pervasive alteration of all preceding carbonate components (including *Cloudina* skeletons (CS) and AC) occurred prior to precipitation of C1c, or that the fluid from which C1c precipitated was responsible for dissolution of pre-existing cements. Alternatively, multiple fluid generations may have promoted alteration prior to growth of C1c within the shallow burial environment. However the observation that pervasively recrystallized CS are occasionally characterised by patchy bright luminescence, indicative of activation by at least moderately elevated Mn, supports the inference that CS were altered by the fluids responsible for the precipitation of C1b, or later alteration of C1b and associated Mn remobilisation.

The final blocky calcite (C2) is length-slow, with an equant form. This is typical of crystal growth in pore waters where Mg/Ca is low, and suggests a burial origin. This cement occludes all remaining pore space. The Sr concentration in C2 is significantly elevated, which likely reflects the relatively low degree of alteration following total pore occlusion.

Cloudina skeleton (CS), thrombolite, and calcite spar cement (C2) show a narrow range of $\delta^{13}C_{PDB}$ from 1.67 to 2.36‰ (mean 2.10‰), and $\delta^{18}O_{PDB}$ from −9.94 to −4.09‰ (mean −7.37‰). Acicular

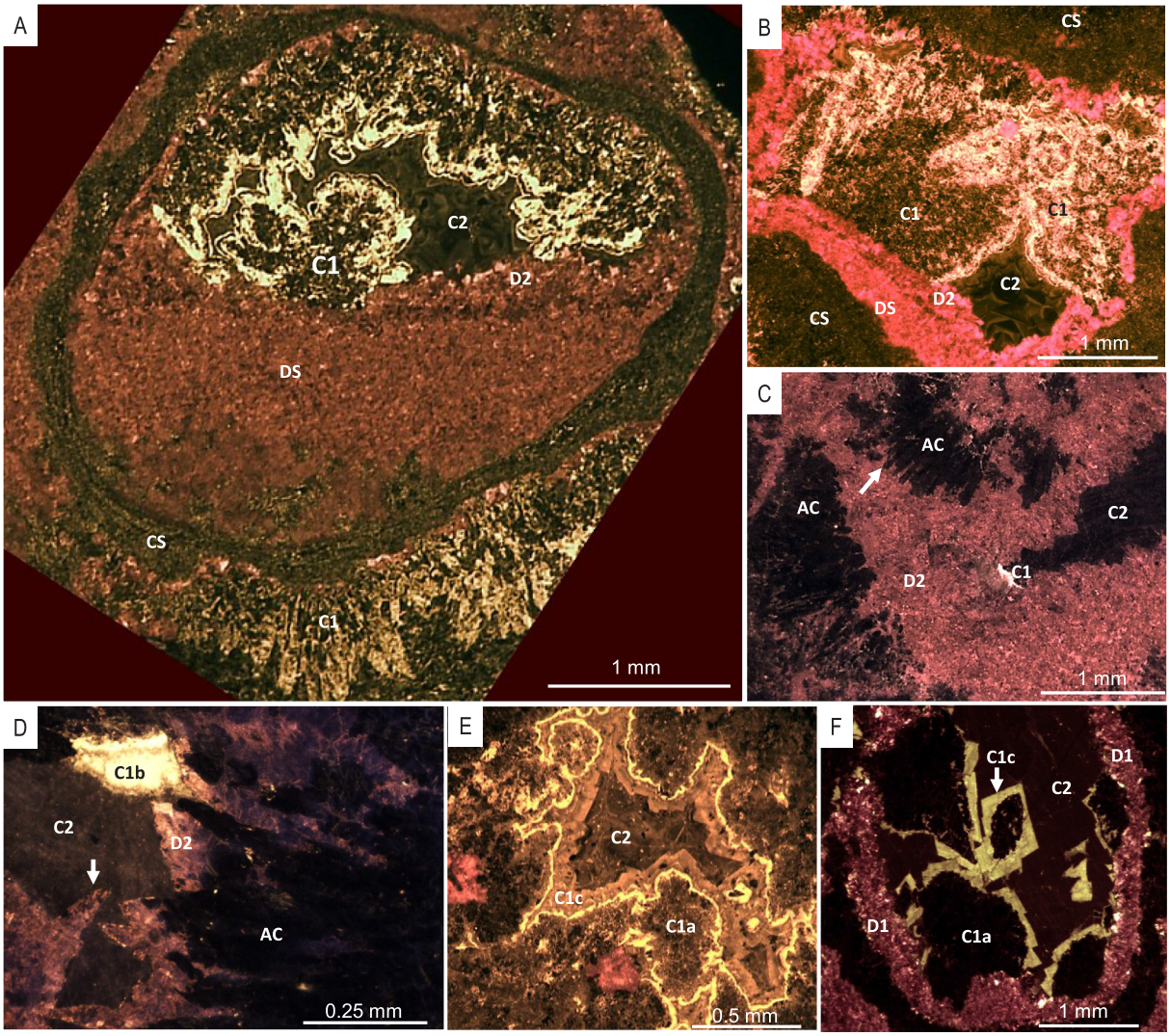

Fig. 7. Cathodoluminescence photomicrographs of cements. (A) Recrystallised *Cloudina* skeleton partially filled with dull luminescent dolomitised geopetal sediment, successively encrusted by dolomite cement and brightly luminescent fibrous calcite cement. The remaining pore space is occluded by dull luminescent calcite. (B) Successive cements within pore space invariably follow the sequence: dull luminescent isopachous dolomite cement (Fe-rich, Mn-poor), non to bright luminescent fibrous calcite cement (Mn-rich, Fe poor), and finally dull luminescent blocky calcite (Fe and Mn-poor). (C) Non-luminescent fibrous acicular cement (Fe and Mn poor) is encrusted by an isopachous, heavily altered dolomite cement (Fe rich, Mn poor), the remaining pore space is lined by a thin, brightly luminescent Mn-rich calcite and finally non-luminescent Fe and Mn-poor calcite. (D) Fibrous acicular cement locally shows evidence for partial dolomitization (arrowed). (E) Fibrous C1 cement is locally overgrown by limpid cement of moderate luminescence (C1c) prior to pore occlusion by non-luminescent blocky calcite (C2). (F) C1c precipitated on C1(a/b) epitaxially.

cement (AC) shows a slightly wider range of $\delta^{13}C_{PDB}$ from 1.15 to 3.02‰ (mean 2.49‰), and $\delta^{18}O_{PDB}$ from −10.99 to −6.63‰ (mean −8.40‰). This is not surprising as the aragonite has converted to calcite during diagenesis, either in meteoric waters or at higher temperatures during burial, producing lighter oxygen isotopic compositions. There is a notable positive correlation between $\delta^{13}C_{carb}$ and $\delta^{18}O_{carb}$ for AC, but data are too sparse to detect trends in any other calcitic components. This strongly suggests that the AC cements have been subject to progressive diagenetic alteration. The isotope values alone do not rule out the influence of either meteoric or burial diagenesis. The C2 cements do not, however, show the very light $\delta^{18}O_{PDB}$ values indicative of late burial diagenesis, but data points are sparse and values may be also influenced by the buffering effects of the increasingly higher $\delta^{18}O$ values in the pore fluid through time due to rock-water interaction.

In summary, the CL and Fe-Mn abundance data indicate that cements were precipitated under variable water column redox conditions: originally non-luminescent acicular cement (AC) in oxic conditions (with no Fe and Mn), and then non to brightly luminescent fibrous and columnar, inclusion-rich calcite (C1) was first precipitated under dominantly oxic (C1a) (low Fe and Mn) and then dominantly low oxygen manganous (C1b) conditions (low Fe and high Mn). The patchy luminescence of C1a suggests some recrystallization, possibly from an HMC precursor. The non-luminescent blocky calcite (C2) grew under oxic conditions probably during shallow burial. $\delta^{13}C_{PDB}$ and $\delta^{18}O_{PDB}$, for carbonate components occupy similar values, and do not rule out the influence of either meteoric or burial diagenesis.

5.2. Origin of dolomite cements

We infer that the elevated iron concentrations found in dolomitised *Cloudina* individuals (D1), geopetal dolomicrite sediment, and dolomite cements D2 were introduced during the dolomitisation process and were not a pre-existing feature of any of the precursors. Therefore, constraining the timing of dolomitisation is key to understanding the evolution of redox conditions.

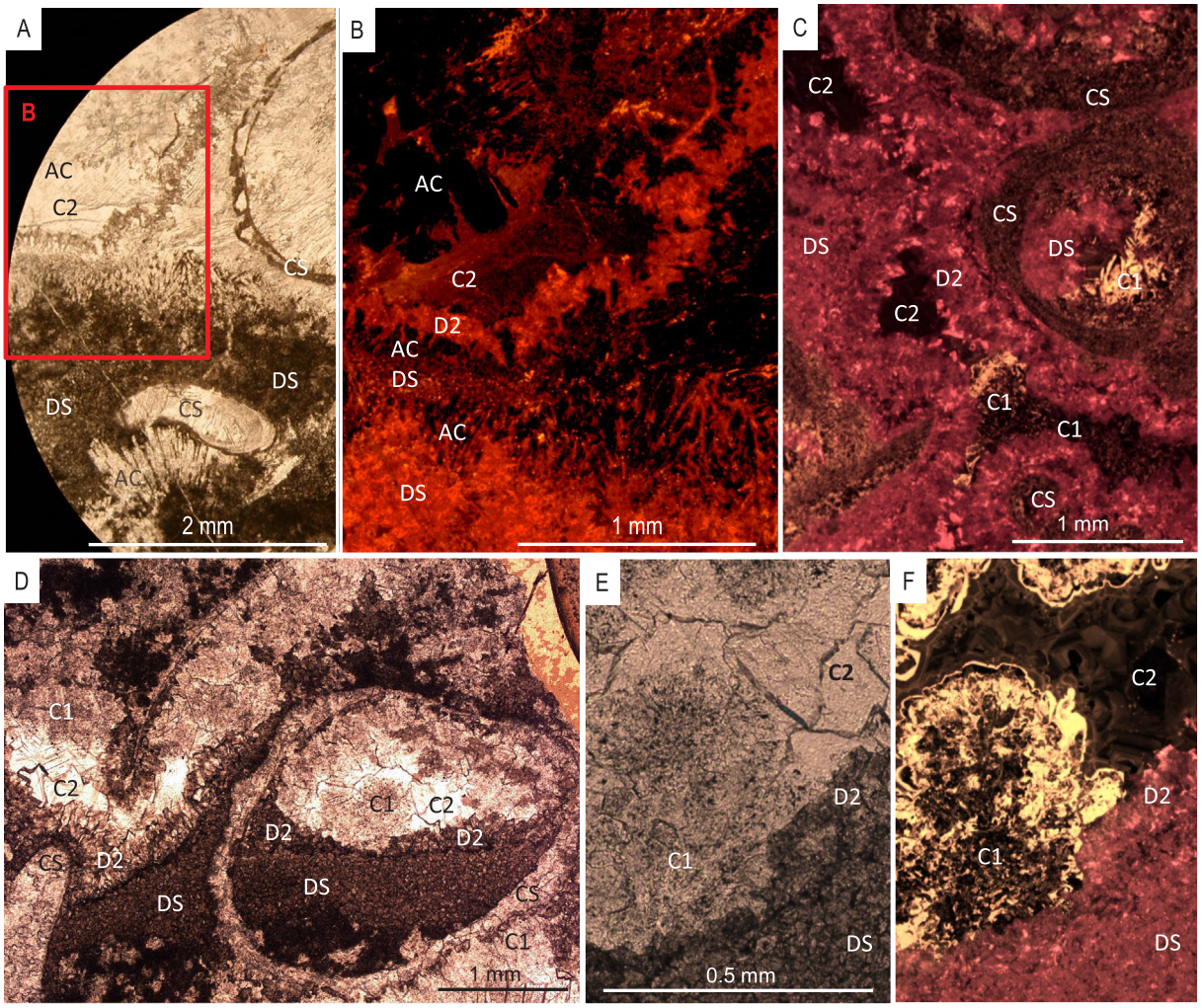

Fig. 8. Photomicrographs of cements. (A) Transmitted light photomicrographs of cements in plane polarised light. Image clearly shows cement stratigraphy with repeated burial of acicular cement by dolomitised sediment, which is then capped by a crust of dolomite cement with length-fast character. (B) enlarged cathodoluminescence image of boxed area in (A). Early acicular marine cement repeatedly nucleates on top of dolomitised sediment and is finally encrusted by an isopachous dolomite cement (D1). Final pore space is occluded by non-luminescent calcite cement. (C) Cathodoluminescence photomicrograph showing well-developed isopachous dolomite cement (D2) encrusting *Cloudina* skeletons. Remaining pore space is occluded successively by non-brightly luminescing fibrous calcite (C1) and finally non-luminescent blocky calcite (C2). (D) Transmitted light photomicrograph in plane polarised light. *Cloudina* reef framework with dolomitised geopetal sediment fill encrusted by dolomite cement (D2). Remaining pore space is occluded by two generations of calcite cement, inclusion-rich C1 and blocky, inclusion-poor C2. (E) Transmitted light photomicrograph in plane polarised light showing cloudy, inclusion-rich nature of fibrous, calcite cement (C1), (F) Cathodoluminescence photomicrograph of C1.

As a result of the slow kinetics of dolomite formation at temperatures less than 40 °C (Arvidson and Mackenzie, 1999), it has been proposed that under near-normal sea water conditions unstable, precursor, Ca–Mg carbonate phases form, such as very high-Mg calcite (VHMC). Prior to dolomite formation VHMC, over decades or more, may become more ordered dolomite through dissolution and re-precipitation (Kaczmarek et al., 2017). This progression is common in natural settings where higher burial temperatures and long time periods overcome kinetic barriers to dolomite formation (Kaczmarek et al., 2017).

High magnesium calcite (HMC) has previously been inferred for the mineralogy of original *Cloudina* shell material at Driedoornvlagte and has similarly been suggested to provide a localised source of Mg^{2+} required during subsequent diagenetic dolomitisation (Grant, 1990), forming the D1 cement. Early dolomitisation of a HMC precursor cement is similarly inferred for D2, as neither the preceding acicular cement, nor later calcite cements, are dolomitised. This is supported by the observation that some of the D2 cement crystals exhibit the classic HMC form with a length-fast character and acute rhombic crystal terminations (Figs. 7D, 8F).

The presence of dissolution suggests that precipitation took place under variable conditions which may have included multiple fluid alteration stages accompanied by possible changes in carbonate saturation state. Dolomite cement increases in volume from the base to the top of each assemblage, and is controlled by the available pore space for precipitation after synsedimentary acicular cement growth.

There is a complete overlap in the $\delta^{18}O_{carb}$ of dolomitic and calcitic components, but dolomitic components reach slightly lower values. The most depleted $\delta^{13}C_{carb}$ values are also associated with dolomite (from −0.29 to 2.62‰) compared to the calcitic components (from 1.15 to 3.02‰) (Fig. 10). There is a notable positive correlation between $\delta^{13}C_{carb}$ and $\delta^{18}O_{carb}$ within the dolomite samples, which strongly suggests the influence of diagenetic alteration which progressively lowered values.

Low oceanic oxygen levels in the Neoproterozoic might provide a control on marine dolomite precipitation by promoting microbial reactions such as methanogenesis or sulphate reduction (Burns et al., 2000). The carbon isotopic composition of dolomite may also reveal the

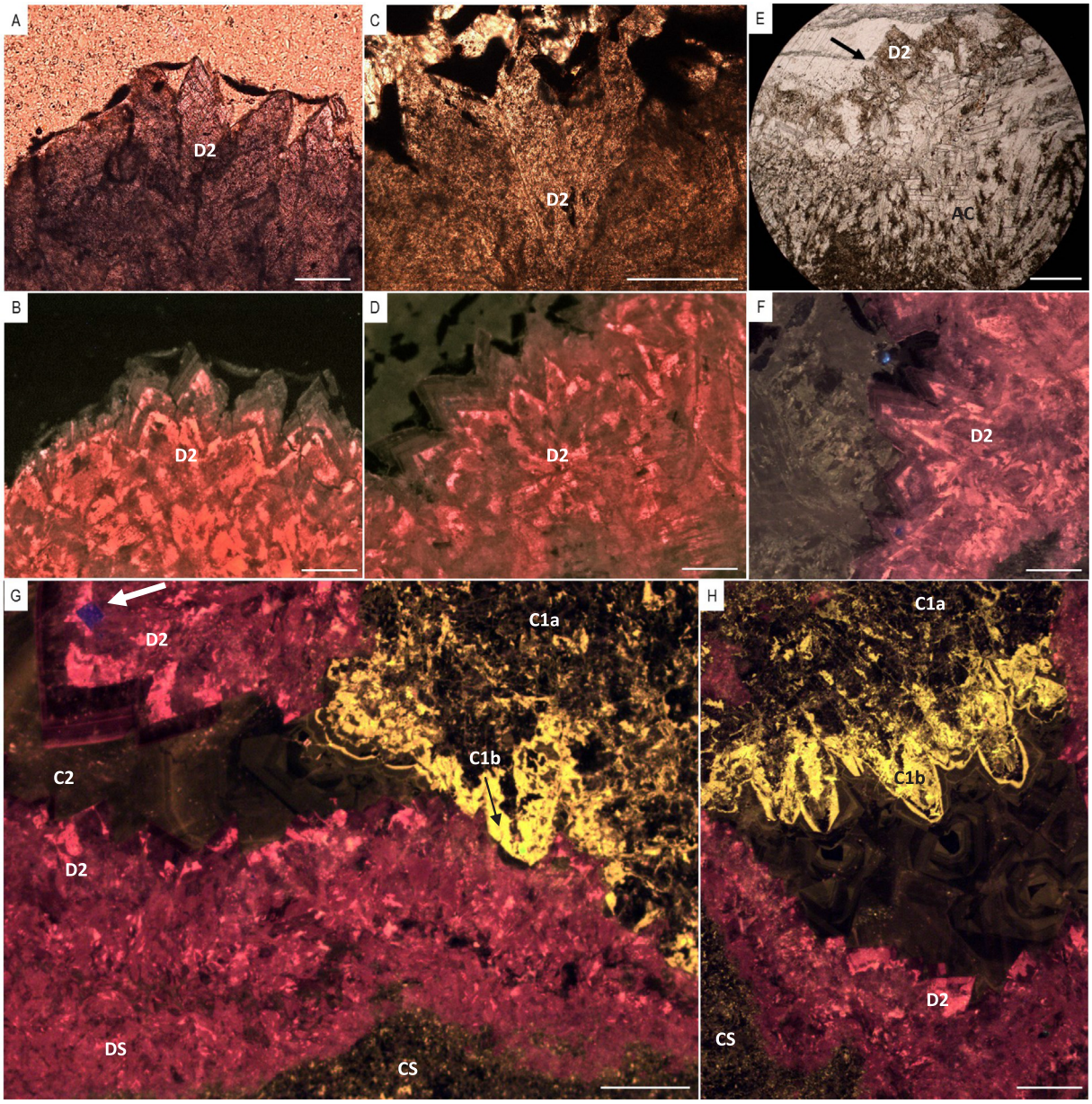

Fig. 9. Photomicrographs of Dolomite cement (D2) (A-F) and calcite (C1) (G, H) cements. A and C are plane polarised light images of B and D respectively. B, D, F, G: Localised, fine CL zonation in D2 cement. (E) Dissolution of crystal terminations (arrow); (F) Acute rhombic terminations typical of high-Mg calcite when the plane of the thin section bisects the D2 cement parallel (/near-parallel) to the c-axis. Final growth zones show the most dull luminescence; (G) Fluorite is rarely present as an accessory mineral within D2 cement (arrow). (H), Fibrous columnar, scalenohedral nature of C1 when plane of thin section bisects the crystal parallel to the c-axis. All scale bars are 0.1 mm.

degree to which dolomitization was controlled by bacterial processes within anoxic pore fluids. Using carbon isotope signatures, both sulphate reduction and methanogenesis have been evoked to explain precipitation of transient dolomite cements in Holocene shallow marine carbonate platforms (Teal et al., 2000) and for marine dolomite cements of the Cryogenian Oodnaminta Reef complex (Hood et al., 2011; Hood and Wallace, 2012). Notwithstanding the very low quantities of pyrite (< 0.1 wt%), the light carbon isotope signature of some combined dolomite sediment and dolomite cement samples relative to all other components supports a role for bicarbonate produced by a variety of early diagenetic organic matter remineralisation reactions.

Dolomitisation and dolomite formation in the modern is largely restricted to shallow sediments that are frequently subject to evaporative conditions (Machel, 2004). Though reef growth of Unit 3 m is inferred to have occurred above fair weather wave base, there are no features of subaerial exposure or evaporative conditions but rather transgression and deepening leading to eventual swamping by basinal shales of the Urikos Member (Adams et al., 2004). Given the high porosity of the reef system, pore spaces were likely connected to the overlying water column prior to inundation by Urikos sediments. Circulation through the sediment of considerable volumes of seawater is required for dolomite formation, driven by tidal plumbing, wind generated currents and storms. We infer that sediment porosity was sufficiently high to have maintained interstitial seawater circulation and dolomite precipitation. Furthermore, precipitation of the dolomite cement was likely promoted by sustained, elevated pore water alkalinity, where Mg was sourced from seawater and possibly aragonite neomorphism (although this would most likely have occurred mainly during burial), as well as localised sulphate reduction. Elevated Fe also supports a role for anoxia. These conditions, coupled with unstable and

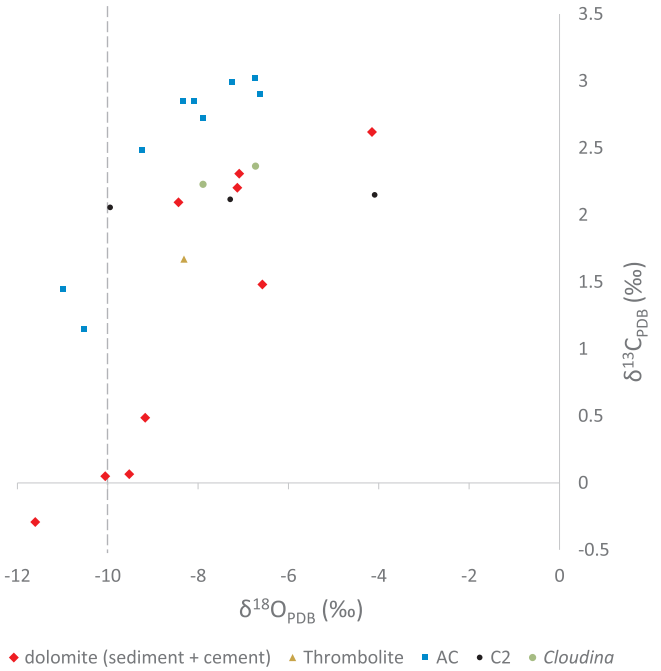

Fig. 10. $\delta^{18}O$ and $\delta^{13}C$ cross plot for separated skeletal, and calcite and dolomite components.

reactive precursor phases such as HMC, would further enhance the dolomitization potential of fluids sourced from seawater (Corsetti et al., 2006).

The geopetal sediment likely acted as a route for dolomitising fluids due to its relatively high permeability and small grain size. But the timing of dolomitisation of the geopetal sediment, HMC *Cloudina* individuals, and inferred HMC precursor cement is difficult to constrain. However the fact that D2 cement crystals largely show a unimodal size distribution is suggestive of a single cementation event (Machel, 2004). Fluorite is a common accessory mineral in dolomite as a consequence of increasing Ca^{2+} and decreasing Mg^{2+} (resulting in decay of MgF^{+} complexes) in pore solutions during dolomitisation (Dickson, 1980; Möller et al., 1980). We infer that dolomitisation may have been enhanced either very early via upwelling of deeper, ferruginous seawater prior to inundation by Urikos sediments, or by later fluid remobilisation from adjacent and overlying Urikos Member shales during shallow burial. Dolomitisation would, however, have occurred prior to final occlusion of porosity within the reefs, i.e. prior to the precipitation of the localised epitaxial cement (C1c) and the final pore-occluding cement (C2).

If dolomitisation proceeded during shallow burial, anoxic pore water ferric oxide reduction and remobilisation from overlying shales would have supplied ferrous iron which was incorporated into the dolomite lattice. But the question remains as to whether such shallow burial conditions would have been permissive to growth of the length-fast character as shown in C1(a/b), where elevated Mg/Ca and good connection with overlying seawater is strongly implied. In addition, if growth of the inferred originally HMC C1 cement predated dolomitisation, then why was this cement not also dolomitised?

Iron speciation and Ce/Ce* data strongly suggest local water column conditions to have been variably ferruginous, manganous and oxic (Wood et al., 2015; Tostevin et al., 2016; Bowyer et al., 2017). The simplest explanation for the sequence of inferred redox conditions and associated crystallographic character of carbonate cements is the effect of seawater of changing reduction potential prior to pore water disconnect by deposition of the Urikos Member. In this case, dolomitisation is inferred to have been early, and was catalysed in the presence of ferruginous waters of elevated Mg/Ca, in addition to anoxic microbial activity.

We interpret such a succession of early marine cements in these open reef systems to represent precipitation at either successively deeper positions in the water column or through changing pore water chemistry due to transgression and/or upwelling, from shallow oxic (AC, C1a) through to manganous (C1b). The dolomitized sediment (DS) and associated dolomite crust (D1 and 2) may have formed as a result of a temporary incursion of Mg-rich, anoxic ferruginous waters, combined with sulphate reduction, but this hypothesis remains to be tested. Dissolution is common, suggesting possible changes in the mean carbonate saturation state. These changes in sea water and/or pore fluid chemistry may have been produced by upwelling related to high-frequency cycles of transgression which led to shoaling of the oxycline (Bowyer et al., 2017). This interpretation is supported by the presence of dolomitized sediment at the same horizon in other mid-ramp (Zebra River) and inner-ramp (Omkyk and Zwartmodder) localities. For example, at the inner ramp site Omkyk (Fig. 1A), the in-situ *Namacalathus* assemblages on bedding planes show dolomitisation of surrounding micrite sediment, but retention of limestone within the *Namacalathus* cups (Fig. 3E and F). This coincides with a short-lived anoxic event as revealed by Fe speciation at the MFS of the Upper Omkyk Member (OS2) (Fig. 11A; Bowyer et al., 2017).

6. Conclusions

Ediacaran oceans were probably of high Mg/Ca with a shallow and fluctuating oxic chemocline compared to most of the Phanerozoic. Our cement data are consistent with the interpretation that Nama Group Ediacaran skeletal communities grew in oxic waters but close to the chemocline, with growth terminated by low oxygen, manganous waters that shoaled during late transgressive to early highstand cycles. Encroachment of anoxic, ferruginous waters in shallow environments may have dolomitised sediment and a HMC cement precursor. Dissolution is also common in the paragenetic succession of cements, suggesting changes in the mean carbonate saturation state. We hence hypothesise a model of dynamic redox changes through the Omkyk Member (Fig. 11B–D). The Lower Omkyk (OS1) shows expansion of anoxic waters across the ramp with no recorded benthic biota, but during the Upper Omkyk (OS2), the chemocline occupied a position lower in the water column and skeletal communities grew at Driedoornvlagte, Zebra River and Omkyk within the oxic portion of the water column. At the maximum flooding surface, there was a shoaling of the chemocline, causing termination of communities at Driedoornvlagte and dolomitisation of host sediment and replacement of a HMC cement by iron-rich dolomite.

Growth of major Ediacaran communities in the Nama Group was likely terminated by low-oxygen or anoxic incursions, resulting in extensive dolomitisation. Such communities may therefore have experienced regular devastation, leading to both an observed patchy distribution and limited longevity.

Acknowledgments

F.B. acknowledges NERC (Grant award code NE/L002558/1), A.P. acknowledges support from the University of Edinburgh, and R.W and A.P. from the International Centre for Carbonate Reservoirs and the Daniel Pidgeon Fund of the Geological Society of London. S.W.P. acknowledges support from a Royal Society Wolfson Research Merit Award. We thank Helke Mocke and Charlie Hoffmann of the Geological Survey of Namibia, and the Ministry of Mines and Energy, Namibia. C. Husselman of Driedoornvlagte, A. Horn of Omkyk and Zwartmodder, and L. and G. Fourie of Zebra River, are thanked for access to their farm, and Mike Hall and Chris Haywood for technical support. We thank Ashleigh Hood and an anonymous reviewer for their thoughtful comments.

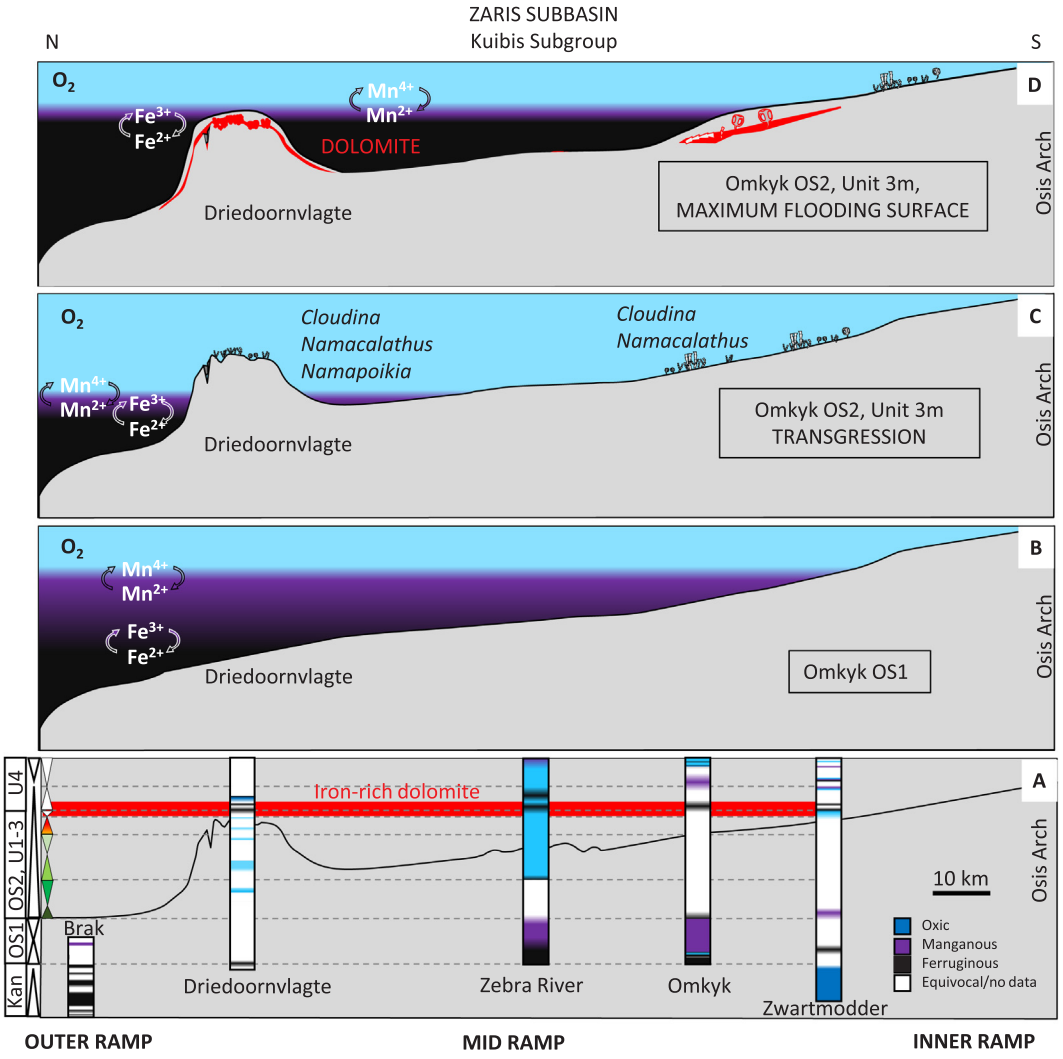

Fig. 11. Simplified cross section of the redox structure of the Zaris Sub-basin during deposition of the Omkyk Member, Kuibis Formation, showing the position of Brak, Driedoornvlagte, Zebra River, Omkyk and Zwartmodder. (A) The evolution of redox structure through the Omkyk Member (from Wood et al., 2015; Tostevin et al., 2016; Bowyer et al., 2017), and the position of the iron-rich dolomite which can be correlated across the basin. Parasequences of OS1 and OS2 are coloured according to Fig. 2 (after Adams et al., 2004, 2005). (B) Lower Omkyk (OS1), showing expansion of anoxic waters across the ramp, with no benthic biota. (C) Upper Omkyk (OS2) transgressive systems tract. *Cloudina, Namacalathus* and *Namapoikia* grew within the oxic portion of the water column but close to the chemocline at Driedoornvlagte, Zebra River and Omkyk. (D) Upper Omkyk (OS2) maximum flooding surface, showing shoaling of the chemocline at the end of transgression, causing termination of benthic community growth and dolomitisation of host sediment and iron-rich dolomite cement.

Appendix A. Supplementary data

Supplementary data associated with this article can be found, in the online version, at http://dx.doi.org/10.1016/j.precamres.2018.05.011.

References

Adams, E.W., Grotzinger, J.P., Watters, W.A., Schroder, S., McCormick, D.S., Al-Siyabi, H.A., 2005. Digital characterization of thrombolite-stromatolite reef distribution in a carbonate ramp system (terminal Proterozoic, Nama Group, Namibia). AAPG Bull. 89, 1293–1318.

Adams, E., Schroder, S., Grotzinger, J.P., McCormick, D.S., 2004. Digital reconstruction and stratigraphic evolution of a microbial-dominated isolated carbonate platform (terminal Proterozoic, Nama Group, Namibia). J. Sediment. Res. 74, 479–497.

Arvidson, R.S., Mackenzie, F.T., 1999. The dolomite problem: control of precipitation kinetics by temperature and saturation state. Am. J. Sci. 299, 257–288.

Barnaby, R.J., Rimstidt, J.D., 1989. Redox conditions of calcite cementation interpreted from Mn and Fe contents of authigenic calcites. Geol. Soc. Am. Bull. 101, 795–804.

Bengtson, S., Zhao, Y., 1992. Predatorial borings in late Precambrian mineralized exoskeletons. Science 257, 367–369.

Berner, R.A., 1975. The role of magnesium in the crystal growth of calcite and aragonite from sea water. Geochim. Cosmochim. Acta 39, 489–504.

Bowyer, F.T., Wood, R.A., Poulton, S.W., 2017. Controls on the evolution of Ediacaran metazoan ecosystems: a redox perspective. Geobiology 15, 516–551.

Brennan, S.T., Lowenstein, T.K., Horita, J., 2004. Seawater chemistry and the advent of calcification. Geology 32, 473–476.

Buatois, L.A., Almond, J., Mángano, M.G., Jensen, S., Germs, G.J.B., 2018. Sediment disturbance by Ediacaran bulldozers and the roots of the Cambrian explosion. Nat. Sci. Rep. 8, 1–9.

Burns, S.J., Mckenzie, J.A., Vasconcelos, C., 2000. Dolomite formation and biogeochemical cycles in the Phanerozoic. Sedimentology 47, 49–61.

Canfield, D.E., Poulton, S.W., Knoll, A.H., Narbonne, G.M., Ross, G., Goldberg, T., Strauss, H., 2008. Ferruginous conditions dominated later Neoproterozoic deep water chemistry. Science 321, 949–952.

Clarkson, M.O., Poulton, S.W., Guilbard, R., Wood, R., 2014. Assessing the utility of Fe/Al and Fe-speciation to record water column redox conditions in carbonate-rich sediments. Chem. Geol. 382, 111–122.

Corsetti, F.A., Kidder, D.L., Marenco, P.J., 2006. Trends in oolite dolomitization across the Neoproterozoic-Cambrian boundary: A case study from Death Valley, California. Sed. Geol. 191, 135–150.

Davies, G.R., 1977. Former magnesian calcite and aragonite submarine cements in upper Paleozoic reefs of the Canadian Arctic: a summary. Geology 5, 11–15.

Della Porta, G., Webb, G.E., McDonald, I., 2015. REE patterns of microbial carbonate and cements from Sinemurian (Lower Jurassic) siliceous sponge mounds (Djebel Bou Dahar, High Atlas, Morocco). Chem. Geol. 400, 65–86.

Dibenedetto, S., Grotzinger, J., 2005. Geomorphic evolution of a storm dominated carbonate ramp (c. 549 Ma), Nama Group, Namibia. Geol. Mag. 142 (583), 604.

Dickson, J.A.D., 1965. A modified staining technique for carbonates in thin section. Nature 205 587-587.

Folk, R.L., 1974. The natural history of crystalline calcium carbonate: effect of magnesium content and salinity. J. Sediment. Res. 44, 40–53.
Folk, R.L., Land, L.S., 1975. Mg/Ca ratio and salinity: two controls over crystallization of dolomite. AAPG Bull. 59, 60–68.
Grant, S.W.F., 1990. Shell structure and distribution of *Cloudina*, a potential index fossil for the terminal Proterozoic. Am. J. Sci. 290A, 261–294.
Grotzinger, J.P., Miller, R McG., 2008. The Nama Group. In: Miller, R.McG. (Ed.), The Geology of Namibia. Geological Survey of Namibia, pp. 13.229–13.272.
Grotzinger, J.P., Bowring, S.A., Saylor, B.Z., Kaufman, A.J., 1995. Biostratigraphic and geochronologic constraints on early animal evolution. Science 270, 598–604.
Grotzinger, J.P., Adams, E.W., Schroeder, S., 2003. Microbial–metazoan reefs of the terminal Proterozoic Nama Group (*c*. 550–543 Ma), Namibia. Geol. Mag. 142, 499–517.
Grover, G., Read, J., 1983. Paleoaquifer and deep burial related cements defined by regional cathodoluminescent patterns, Middle Ordovician carbonates, Virginia. AAPG Bull. 67, 1275–1303.
Habermann, D., Neuser, R.D., Richter, D.K., 1996. REE-activated cathodoluminescence of calcite and dolomite: high-resolution spectrometric analysis of CL emissions (HRS-CL). Sed. Geol. 101, 1–7.
Habermann, D., Neuser, R.D., Richter, D.K., 1998. Low limit of Mn^{2+}-activated cathodoluminescence of calcite: state of the art. Sed. Geol. 116 (13), 24.
Hardie, L.A., 2003. Secular variations in Precambrian seawater chemistry and the timing of Precambrian aragonite seas and calcite seas. Geology 31, 785–788.
Hood, A.V.S., Wallace, M.W., Drysdale, R.N., 2011. Neoproterozoic aragonite dolomite seas? Widespread marine dolomite precipitation in Cryogenian reef complexes. Geology 39, 871–874.
Hood, A.V.S., Wallace, M.W., 2012. Synsedimentary diagenesis in a Cryogenian reef complex: ubiquitous dolomite precipitation. Sed. Geol. 255–256, 56–71.
Hood, A.V.S., Wallace, M.W., 2015. Extreme ocean anoxia during the Late Cryogenian recorded in reefal carbonates of Southern Australia. Precambr. Res. 261, 96–111.
Hood, A.V.S., Wallace, M.W., 2018. Neoproterozoic marine carbonates and their paleoceanographic significance. Global Planet. Change 160, 28–45.
Johnston, D.T., Poulton, S.W., Tosca, N.J., O'Brien, T., Halverson, G.P., Schrag, D.P., Macdonald, F.A., 2013. Searching for an oxygenation event in the fossiliferous Ediacaran of northwestern Canada. Chem. Geol. 362, 273–286.
Kaczmarek, S.E., Gregg, J.M., Bush, D.L., Machel, H.G., Fouke, B.W., 2017. Dolomite, Very High-Magnesium Calcite, and Microbes – Implications for the Microbial Model of Dolomitization, vol. 109 SEPM Special Publications Characterization and Modeling of Carbonates – Mountjoy Symposium 1.
Kendall, B., Komiya, T., Lyons, T.W., Bates, S.M., Gordon, G.W., Romaniello, S.J., Jiang, G., Creaser, R.A., Xiao, S., McFadden, K., Sawaki, Y., Tahata, M., Shu, D., Han, J., Li, Y., Chu, X., Anbar, A.D., 2015. Uranium and molybdenum isotopeevidence for an episode of widespread ocean oxygenation during the late Ediacaran Period. Geochim. Cosmochim. Acta 156, 173–193.
Knoll, A.H., 2003. Biomineralisation and evolutionary history. Rev. Miner. Geochem. 54, 329–356.
Lumsden, D.N., Chimahusky, J.S., 1980. In: Relationship Between Dolomite Nonstoichiometry and Carbonate Facies Parameters. SEPM Special Publication, pp. 123–137.
Lyons, T.W., Reinhard, C.T., Planavsky, N.J., 2014. The rise of oxygen in Earth's early ocean and atmosphere. Nature 506, 307–315.
Machel, H.G., 2004. Concepts and models of dolomitization: a critical reappraisal. Geol. Soc., London, Spec. Publ. 235, 7–63.
Mason, R.A., Mariano, A.N., 1990. Cathodoluminescence activation in manganese-bearing and rare earth-bearing synthetic calcites. Chem. Geol. 88, 191–206.
Mehra, A., Maloof, A., 2018. Multiscale approach reveals that Cloudina aggregates are detritus and not in situ reef constructions. PNAS, 201719911.
Möller, P., Schulz, S., Jacob, K.H., 1980. Formation of fluorite in sedimentary basins. Chem. Geol. 31, 97–117.
Nothdurft, L.D., Webb, G.E., Kamber, B.S., 2004. Rare earth element geochemistry of Late Devonian reefal carbonates, Canning Basin, Western Australia: confirmation of a seawater REE proxy in ancient limestones. Geochim. Cosmochim. Acta 68, 263–283.
Penny, A.M., Wood, R.A., Curtis, A., Bowyer, F., Tostevin, R., Hoffman, K.H., 2014. Ediacaran metazoan reefs from the Nama Group, Namibia. Science 344, 1504–1506.
Peters, S.E., Gaines, R.R., 2012. Formation of the 'Great Unconformity' as a trigger for the Cambrian explosion. Nature 484, 363–366.
Planavsky, N.J., McGoldrick, P., Scott, C.T., Li, C., Reinhard, C.T., Kelly, A.E., Chu, X., Bekker, A., Love, G.D., Lyons, T.W., 2011. Widespread iron-rich conditions in the mid-Proterozoic ocean. Nature 477, 448.
Poulton, S.W., Canfield, D.E., 2011. Ferruginous conditions: a dominant feature of the ocean through Earth's history. Elements 7, 107–112.
Saylor, B.Z., Grotzinger, J.P., Germs, G.J.B., 1995. Sequence stratigraphy and sedimentology of the Neoproterozoic Kuibis and Schwarzrand Subgroups (Nama Group), southwestern Namibia. Precambr. Res. 73, 153–171.
Saylor, B.Z., Kaufman, A.J., Grotzinger, J.P., Urban, F., 1998. A composite reference section for terminal Proterozoic strata of southern Namibia. J. Sediment. Res. 68, 1223–1235.
Schmitz, M.D., 2012. Radiogenic isotope geochronology. In: Gradstein, F.M., Ogg, J.G., Schmitz, M.D., Ogg, G.M. (Eds.), Geologic Time Scale 2012. Elsevier, pp. 115–126.
Sibley, D.F., Gregg, J.M., 1987. Classification of dolomite rock textures. J. Sediment. Res. 57, 967–975.
Smith, O.A., 1998. Terminal Proterozoic Carbonate Platform Development: Stratigraphy and Sedimentology of the Kuibis Subgroup (ca. 550–548 Ma), Northern Nama Basin, Namibia (Unpublished Masters Thesis). Massachusetts Institute of Technology.
Spence, G.H., Le Heron, D.P., Fairchild, I.J., 2016. Sedimentological perspectives on climatic, atmospheric and environmental change in the Neoproterozoic Era. Sedimentology 63, 253–306.
Sperling, E.A., Wolock, C.J., Morgan, A.S., Gill, B.C., Kunzmann, M., Halverson, G.P., Macdonald, F.A., Knoll, A.H., Johnston, D.T., 2015a. Statistical analysis of iron geochemical data suggests limited late Proterozoic oxygenation. Nature 523, 451–454.
Sperling, E.A., Carbone, C., Strauss, J.V., Johnston, D.T., Narbonne, G.M., Macdonald, F.A., 2015b. Oxygen, facies, and secular controls on the appearance of Cryogenian and Ediacaran body and trace fossils in the Mackenzie Mountains of northwestern Canada. Geol. Soc. Am. Bull. 128, 558–575.
Teal, C.S., Mazzullo, S.J., Bischoff, W.D., 2000. Dolomitization of Holocene shallow-marine deposits mediated by sulphate reduction and methanogenesis in normal-salinity seawater, northern Belize. J. Sediment. Res. 70, 649–663.
Tostevin, R., Wood, R.A., Shields, G.A., Poulton, S.W., Guilbaud, R., Bowyer, F., Penny, A.M., He, T., Curtis, A., Hoffman, K.H., Clarkson, M.O., 2016. Low-oxygen waters limited habitable space for early animals. Nat. Commun. 7, 12818.
Tucker, M.E., 1982. Precambrian dolomites: petrographic and isotopic evidence that they differ from Phanerozoic dolomites. Geology 10, 7–12.
Tucker, M.E., 1983. Diagenesis, geochemistry, and origin of a Precambrian dolomite: the Beck Spring Dolomite of eastern California. J. Sediment. Res. 53, 1097–1119.
Wallace, M.W., Shuster, A., Greig, A., Planavsky, N.J., Reed, C.P., 2017. Oxygenation history of the Neoproterozoic to early Phanerozoic and the rise of land plants. Earth Planet. Sci. Lett. 466, 12–19.
Whittaker, S.G., James, N.P., Kyser, T.K., 1994. Geochemistry of synsedimentary cements in Early Cambrian reefs. Geochim. Cosmochim. Acta 58, 5567–5577.
Wood, R.A., Curtis, A., 2015. Extensive metazoan reefs from the Ediacaran Nama Group, Namibia: the rise of benthic suspension feeding. Geobiology 13, 112–122.
Wood, R.A., Grotzinger, J.P., Dickson, J.A.D., 2002. Proterozoic modular biomineralized metazoan from the Nama Group, Namibia. Science 296, 23836.
Wood, R.A., Poulton, S.W., Prave, A.R., Hoffmann, K.-H., Clarkson, M.O., Guilbaud, R., Lyne, J.W., Tostevin, R., Bowyer, F., Penny, A.M., Curtis, A., Kasemann, S.A., 2015. Dynamic redox conditions control late Ediacaran ecosystems in the Nama Group, Namibia. Precambr. Res. 261, 252–271.
Wood, R.A., Zhuravlev, A.Y., Sukhov, S.S., Zhu, M., Zhao, F., 2016. Demise of Ediacaran dolomitic seas marks widespread biomineralization on the Siberian Platform. Geology 45, 27–30.
Wood, R.A., Curtis, A., Penny, A., Zhuravlev, A.Y., Curtis-Walcott, S., Iipinge, S., Bowyer, F., 2017. Flexible and responsive growth strategy of the Ediacaran skeletal *Cloudina* from the Nama Group, Namibia. Geology 45, 259–262.